JGR Earth Surface

RESEARCH ARTICLE
10.1029/2025JF008616

**Special Collection:**
Aeolian-Fluvial Interactions across the Solar System

**Key Points:**

- Ripple celerity exhibits a non-linear relationship to shear velocity under strong wind speeds
- Ripple celerity and height respond more quickly to changes in wind speed than ripple wavelength and reorientation
- Aerodynamic roughness is influenced by saltation and ripple height, particularly under stronger winds transitioning to a collisional regime

**Supporting Information:**

Supporting Information may be found in the online version of this article.

**Correspondence to:**
J. M. Nield,
J.Nield@soton.ac.uk

**Citation:**
Nield, J. M., Baddock, M. C., Wiggs, G. F. S., Best, J., Christensen, K. T., Delorme, P., et al. (2025). Quantifying the form-flow-saltation dynamics of aeolian sand ripples. *Journal of Geophysical Research: Earth Surface*, *130*, e2025JF008616. https://doi.org/10.1029/2025JF008616

Received 28 MAY 2025
Accepted 3 SEP 2025

**Author Contributions:**
**Conceptualization:** Joanna M. Nield, Matthew C. Baddock, Giles F. S. Wiggs, Jim Best, Kenneth T. Christensen, Andrew Valdez, Martin H. T. Hipondoka, Philippe Claudin
**Data curation:** Joanna M. Nield
**Formal analysis:** Joanna M. Nield
**Funding acquisition:** Joanna M. Nield, Matthew C. Baddock, Giles F. S. Wiggs, Jim Best, Kenneth T. Christensen, Andrew Valdez, Martin H. T. Hipondoka, Philippe Claudin

# Quantifying the Form-Flow-Saltation Dynamics of Aeolian Sand Ripples

**Joanna M. Nield[1], Matthew C. Baddock[2], Giles F. S. Wiggs[3], Jim Best[4], Kenneth T. Christensen[5], Pauline Delorme[6], Andrew Valdez[7], Nathaniel R. Bristow[8], Martin H. T. Hipondoka[9], Daniel P. Goss[1], Natasha S. Wallum[3], and Philippe Claudin[10]**

[1]School of Geography and Environmental Science, University of Southampton, Southampton, UK, [2]Geography and Environment, Loughborough University, Loughborough, UK, [3]School of Geography and the Environment, University of Oxford, Oxford, UK, [4]Departments of Earth Science and Environmental Change, Geography & GIS, and Mechanical Science & Engineering, and Ven Te Chow Hydrosystems Laboratory, University of Illinois Urbana-Champaign, Urbana, IL, USA, [5]Department of Mechanical Engineering, University of Colorado Denver, Denver, CO, USA, [6]Laboratoire de Géologie, Ecole Normale Supérieure, CNRS, PSL Research University, Paris, France, [7]Great Sand Dunes National Park and Preserve, National Park Service, Alamosa, CO, USA, [8]Astrin Biosciences, Inc., Saint Paul, MN, USA, [9]Department of Environmental Science, University of Namibia, Windhoek, Namibia, [10]Physique et Mécanique des Milieux Hétérogènes, CNRS, ESPCI Paris, PSL Research University, Université Paris Cité, Sorbonne Université, Paris, France

**Abstract** Ripples are the most fundamental and ubiquitous aeolian bedforms formed on sandy surfaces, but their small size and fast response times make them inherently difficult to measure. However, these attributes also make ripples excellent flow indicators, and they have been used extensively in planetary locations for this purpose. Here, we use terrestrial laser scanning to measure ripple morphometry and celerity coincidently, as well as saltation height above rippled surfaces. We find that although ripple height and wavelength respond linearly to increased shear velocity, under strong winds ripple celerity exhibits a non-linear increase. This relationship at high wind speeds is also reflected in the response of aerodynamic roughness and saltation dynamics, with a greater maximum saltation height present over ripple lee slopes. Importantly, when using ripple patterns as indicators of flow conditions, celerity or height should be used in preference to wavelength as their dynamics respond faster to changing wind speed. In planetary and stratigraphic settings where measuring celerity is not possible, wavelength should be considered as indicative of consistent wind conditions rather than the full range of sand transporting wind speeds.

**Plain Language Summary** When wind blows over a sandy surface, it typically shapes the sediment into small wave-like patterns known as ripples, which are typically a few millimeters high and tens of centimeters long. These ripples exist in sandy surfaces in coastal and desert areas on Earth as well as other planetary bodies. The height and spacing of ripples change with the velocity of the wind, with both the size and the speed at which the ripples move typically increasing at greater wind speeds. If we can relate the size and speed of ripple movement to wind conditions, then we can potentially infer the winds that formed the ripples by measuring the ripples rather than measuring the wind. This is particularly useful in environments where wind measurements are difficult or impossible. Here, we find that the height and movement (or migration rate) of ripples respond more quickly than the spacing between ripples to increases in wind speed or the orientation of the ripples when the wind direction changes. Consideration of the differing responses of ripple characteristics to changing wind conditions improves our ability to use their shape and size on Earth and other planets to quantify ripple dynamics and their formative winds.

## 1. Introduction

Wind-ripples (also referred to as splash or impact ripples) typically form on sandy surfaces where saltation occurs (Bagnold, 1941; Seppälä & Lindé, 1978). Although ripples are the most common and responsive aeolian bedforms, there has been little research linking their morphological and migratory dynamics to flow or transport drivers (Andreotti et al., 2006; Sherman et al., 2019a). Both modeling and experimental data have elucidated the critical role of grain-bed impacts in driving these dynamics (Anderson, 1987, 1990; Andreotti et al., 2006; Duran et al., 2014; Lester et al., 2025; Yizhaq et al., 2004, 2024), or the role of mid-air particle collisions (Huo et al., 2024) that increase in frequency with increased wind shear velocity and shift the regime of sediment transport to one that is collision-dominated (Pähtz & Durán, 2020, 2023; Ralaiarisoa et al., 2020). While it has

**Investigation:** Joanna M. Nield, Matthew C. Baddock, Giles F. S. Wiggs, Pauline Delorme, Andrew Valdez, Martin H. T. Hipondoka, Daniel P. Goss, Natasha S. Wallum, Philippe Claudin
**Methodology:** Joanna M. Nield, Matthew C. Baddock, Giles F. S. Wiggs, Pauline Delorme, Andrew Valdez, Martin H. T. Hipondoka, Daniel P. Goss, Natasha S. Wallum, Philippe Claudin
**Writing – original draft:** Joanna M. Nield, Matthew C. Baddock, Giles F. S. Wiggs, Jim Best, Kenneth T. Christensen, Pauline Delorme, Andrew Valdez, Nathaniel R. Bristow, Martin H. T. Hipondoka, Daniel P. Goss, Natasha S. Wallum, Philippe Claudin
**Writing – review & editing:** Joanna M. Nield, Matthew C. Baddock, Giles F. S. Wiggs, Jim Best, Kenneth T. Christensen, Pauline Delorme, Andrew Valdez, Nathaniel R. Bristow, Martin H. T. Hipondoka, Daniel P. Goss, Natasha S. Wallum, Philippe Claudin

been established that ripple celerity (or migration rate) increases with faster flow (Andreotti et al., 2006; Duran et al., 2014; Sharp, 1963; Sherman et al., 2019a; Uphues et al., 2022), there is disparity between field and wind tunnel measurements as to the exact rate at which celerity increases (Sherman et al., 2019a).

Studies on the behavior of aeolian ripple morphology typically only consider planform ripple shape and ripple wavelength, or measure a single cross-profile transect line rather than the full 3D ripple form. This limitation is partly due to previous methods being more conducive to analysis in 1 or 2 D, for example, manual measurements such as the shadow method (Werner et al., 1986; Zimbelman et al., 2012), time-lapse photography (Lorenz, 2011; Lorenz & Valdez, 2011; Yizhaq et al., 2008) and laser sheet approaches (Sherman et al., 2019a). While model (Anderson, 1987; Duran et al., 2014) and wind tunnel (Gordon & McKenna Neuman, 2011) results suggest asymmetry in form-flow-transport interactions between the ripple stoss and lee slopes, with a greater concentration of particle collisions and ejections on the ripple stoss, evidence of this behavior in a field context is lacking. Yet, as these universal bedforms are inherently responsive to flow, the ability to reconstruct wind and transport conditions remotely based solely on imagery is enticing, and this would have applications in instances where ripples are used as flow indicators, such as on Mars (Ewing et al., 2017; Hood et al., 2021; Lapotre et al., 2016, 2021; Liu & Zimbelman, 2015; Roback et al., 2022; Rubanenko et al., 2022; Silvestro et al., 2010; Sullivan et al., 2020; Vaz et al., 2023).

Work by Owen (1964) has highlighted the role of the saltation cloud in driving changes in aerodynamic roughness ($z_0$), in contrast to estimates of grain-scale roughness (Nikuradse, 1933). However, ripples are roughness elements and surface roughness also influences aerodynamic roughness (Duran et al., 2019; Field & Pelletier, 2018; Nield et al., 2013; Pelletier & Field, 2016; Sherman & Farrell, 2008). While $z_0$ has been studied extensively in both field (Furtak-Cole et al., 2022; Gillies et al., 2007; King et al., 2006; Lancaster & Baas, 1998; Marticorena & Bergametti, 1995; Raupach, 1992; Raupach et al., 1993; Shao et al., 2015; Wolfe & Nickling, 1996) and wind tunnel experiments (Alvarez et al., 2025; Brown et al., 2008; Cheng et al., 2007; Gillies et al., 2017; King et al., 2008), it is typically parameterized for discrete roughness elements, such as vegetation, rather than continuous and complex rough surfaces such as aeolian ripples.

Terrestrial Laser Scanning (TLS) has revolutionized the way we characterize surface roughness, and several studies have examined the influence of high-resolution surface characterization both with (Field & Pelletier, 2018) and without saltation (Nield et al., 2013; Pelletier & Field, 2016). These studies found that without saltation, aerodynamic roughness is most strongly influenced by surface roughness element height, whereas with saltation, the characteristics of the saltation cloud itself are more important in determining $z_0$. In field environments, it is difficult to determine whether the physical height of a ripple, or the thickness of the saltation layer, has a greater impact on the aerodynamic roughness. Experimental data concerning the multiple scales of aerodynamic roughness on Earth is thus needed urgently (Cooke et al., 2025; Jia et al., 2023) as accurate predictions of aerodynamic roughness are crucial for modeling shear velocity and sediment flux (Farrell & Sherman, 2006).

Here, we employ TLS to quantify, for the first time, both ripple morphology and celerity, as well as the concurrent saltation dynamics, above ripples under varying wind conditions. We elucidate the role of saltation layer depth in ripple adjustment and identify important form-flow-transport interactions close to, and at the same vertical scale as, an erodible sandy surface.

## 2. Study Site and Methods

Four experiments were undertaken on a flat surface within the dry, sand-covered bed of Medano Creek, Great Sand Dunes (GSD) National Park and Preserve, Colorado, USA in 2022 and 2023 (Table 1 and Figure 1) (Nield, Baddock, et al., 2023; Nield, Baddock, & Wiggs, 2025). Rippled surfaces, and above surface saltation, were measured using Leica TLS Scanstations (280 scans) over an approximately 1 m$^2$ area immediately upwind of a Campbell Scientific CSAT3 3D sonic anemometer that measured wind speed and direction at 0.24 m above the surface. The uniform ripple-scale local surface roughness and an unperturbed upwind fetch of 100s m, resulted in the anemometer measurements being from within the subregion of the boundary layer where shear stress is constant. Under the conditions of a fully developed boundary layer, small-scale changes in roughness imposed by the active saltation cloud or ripple height are assumed to not meaningfully alter the location of the anemometer in relation to the constant depth shear layer. Saltation flux measurements were recorded immediately downwind of each square scanned area using: (a) a Sensit-piezoelectric counter (Van Pelt et al., 2009) that was positioned so that the sensor base was flush with the surface and the sensor top extended to a height of 0.014 m above the

**Table 1**
*Details of the TLS Measurements for Each Experimental Set-Up, Great Sand Dunes National Park and Preserve, USA*

| Set-up | Date | Leica instruments | Number of scans | TLS head height (m) | Distance to ripple patch from TLS head (m) | Mean $u_*$ (m/s) | Standard deviation of $u_*$ (m/s) | Initial wind direction (°) |
|---|---|---|---|---|---|---|---|---|
| 1 | 5th April 2022 | P20 | 62 | 1.86 | 7.7 | 0.38 | 0.078 | 253 |
| | | P50 | 59 | 1.87 | 7.9 | | | |
| 2 | 30th March 2023 | P50 | 48 | 1.85 | 8.2 | 0.54 | 0.063 | 53 |
| 3 | 3rd April 2023 | P50 | 49 | 1.81 | 7.9 | 0.53 | 0.054 | 220 |
| 4 | 4th April 2023 | P50 | 62 | 2.03 | 7.5 | 0.41 | 0.075 | 245 |

surface, and (b) Wenglor YH03PCT8 optical gate sensors (Hugenholtz & Barchyn, 2011) at heights of 0.02 and 0.05 m (Figure 1a). The measurement duration was 3 or 1.5 min for weaker and stronger winds, respectively. Saltation heights were calculated as mean maximum heights detected by the TLS following the methods of Nield and Wiggs (2011), and differ from heights derived from exponential fits of flux curves (e.g., Ho et al., 2011; Martin & Kok, 2017). Further details on the data processing methods are given in Supporting Information S1 and are similar to those presented in Delorme et al. (2023).

Each approximately 1 × 1 m rippled surface was divided into 0.002 m transects parallel to the wind direction. Ripple heights were calculated for each transect using the zero-upcrossing method (Davis et al., 2004; Goda, 2000; Martin & Jerolmack, 2013). Ripple wavelengths and celerities were calculated for each transect and transect pair, respectively, using the Matlab cross covariance function. Checks were performed to ensure that the distance that the ripples migrated between scans was less than one bedform wavelength. Bulk relationships of ripple celerity, height and wavelength were calculated using data that had a variation in wind direction of less than 15° from the initial direction of ripple migration.

Previous studies have estimated sediment transport via ripple dynamics through ripple celerity, $c_r$, and either a ripple wavelength, $\lambda_r$ -derived transport flux, $q_l \propto c_r \lambda_r$ (Duran et al., 2014), or a ripple height, $h_r$ -derived transport flux, $q_h \propto c_r h_r$ (Jerolmack et al., 2006). We compare our field measurements of sediment flux to relative ripple-derived flux to examine which ripple metric is a better indicator of flux.

We identified ripple crests using the Matlab edge detection algorithm over the gradient of the surface using the Canny algorithm, followed by deblurring and selection of lines that were above a mean height over the surrounding 0.5 × 0.5 m area, similar to methods used to identify dune crests by Daynac et al. (2024) and Hugenholtz

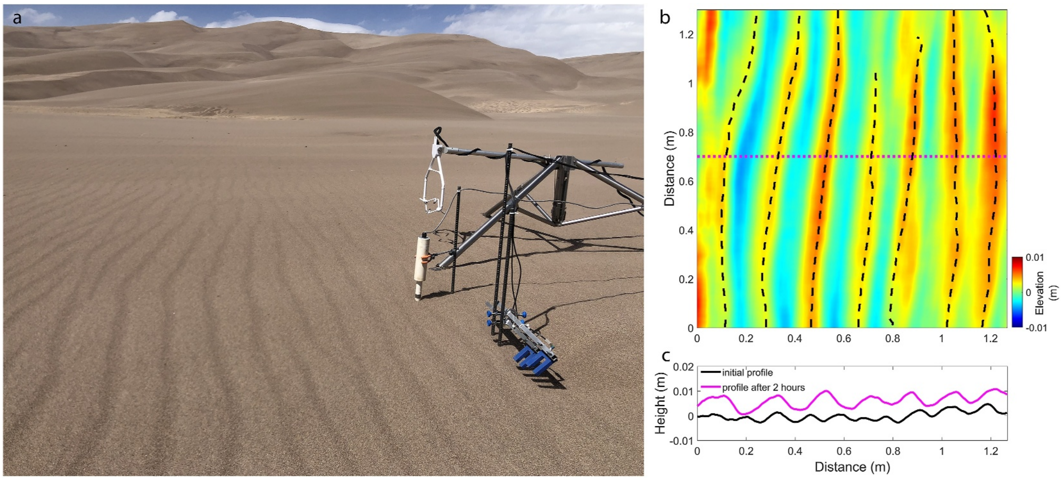

**Figure 1.** (a) Field site set-up at Great Sand Dunes National Park and Preserve on 3rd April 2023. Wind direction from left to right. (b) Example of rippled surface measured on 30th March 2023, with black dashed lines being the identified crest orientations and the magenta dotted line showing the location of the ripple cross sections (c).

**Table 2**
*Details of the TLS Measurements for Additional Measurements in the Huab Valley, Namibia*

| Dune type | Date | Leica instruments | Number of scans | TLS head height (m) | Distance to ripple patch from TLS head (m) | Mean $u_*$ (m/s) | Standard deviation of $u_*$ (m/s) | Anemometer type | Grain size (μm) |
|---|---|---|---|---|---|---|---|---|---|
| Barchan | 6th September 2014 | P20 | 25 | 1.96 | 13 | 0.29 | 0.013 | 3D sonic (0.5 m above surface) | 341 |
| Dome | 22nd September 2016 | P20 | 61 | 1.78 | 5 | 0.32 | 0.021 | Cup (0.24 m above surface) | 402 |
| Dome | 8th September 2018 | P20 | 18 | 1.71 | 7 | 0.26 | 0.011 | Cup (0.24 m above surface) | 402 |

and Barchyn (2010). Crests were then classified as mature if their length was >90% of the measured surface width (i.e., 0.9 m). Lags in ripple responses to changes in wind conditions were calculated using cross-covariance.

Additional measurements (104 scans) were collected on flat crestal areas of barchan and dome dunes in the Huab Valley, Skeleton Coast, Namibia using the same TLS methodology for ripple morphometry, and either 3D sonic or cup anemometers for mean wind speed measurements only and $z_0$ from the literature to estimate $u_*$ (Table 2; Text S1 in Supporting Information S1) (Nield, Wiggs, et al., 2023). Celerity and height data from Oceano Dunes (Sherman et al., 2019b), reported in Sherman et al. (2019a), were also used as a comparator data set as these were collected using a methodology similar to our own, including the use of a 3D sonic anemometer to calculate shear velocity ($u_*$) and a single laser to measure topography. While Sherman et al. (2019b) also reported wavelength data, this did not use the same laser technique employed herein, and thus this part of their data set is not directly comparable to the present paper. Both the Huab and Oceano data supplement our main GSD data set as they were collected at lower shear velocities. Where multiple field site data are used, we have normalized the data to account for grain sizes.

Field quantification of aerodynamic roughness, $z_0$, was undertaken using the Law-of-the-Wall from measurements of Reynolds stress derived $u_*$, and the mean velocity measured at a height of 0.24 m (van Boxel et al., 2004). These measurements were compared to standard empirical relationships between $z_0$ and $u_*$ using the Bagnold roughness law (e.g., Creyssels et al., 2009; Duran et al., 2011; Valance et al., 2015), Equation 1 (where $z_f$ is the focus height, $\kappa$ is the von Kármán constant and $u_f$ is the wind velocity at $z_f$), and a Charnock type model (e.g., Sherman & Farrell, 2008), Equation 2, where $C$ is the Charnock constant and $g$ is gravitational acceleration.

$$z_0 = z_f \exp\left(\frac{-\kappa u_f}{u_*}\right) \tag{1}$$

$$z_0 = \frac{C u_*^2}{g} \tag{2}$$

The relationship between $z_0$ and the surface elevation profile was also characterized in the absence of saltation using the empirical model of Nield et al. (2013). In this case, Jia et al. (2023) found that ripple scale roughness in the absence of saltation should be within the transition between a smooth (Nikuradse, 1933) and rough (Flack & Schultz, 2010) roughness regime, while the presence of saltation moves the system to a rough regime.

## 3. Results and Discussion

### 3.1. Shear Velocity Drives Ripple Height, Wavelength and Celerity

In general, we find that ripple celerity, wavelength and height all increase with increasing shear velocity (Figure 2). The mean ripple index ($\lambda_r/h_r$) within our time averaged data sets remains constant (mean = 41, standard deviation = 2.4). Similar to previous studies that measured ripple dynamics at low values of shear velocity (<2.5 $u_{*t}$) (Duran et al., 2014; Sherman et al., 2019a), we find a linear relationship between $u_*$ and both ripple height and wavelength across a wider range of $u_*$ ($1 < u_{*t} < 3.5$, Figures 2b and 2c). However, using this greater range of $u_*$, which was not accounted for in the previous studies of Duran et al. (2014) and Sherman et al. (2019a), our data also identify a non-linear relationship between $u_*$ and ripple celerity (Figure 2a). The reasons for this are not clear. However, the flattening of ripples under strong winds has been noted by other researchers (Bagnold, 1941; Sharp, 1963) and it is possible that under stronger winds, the increased height of the

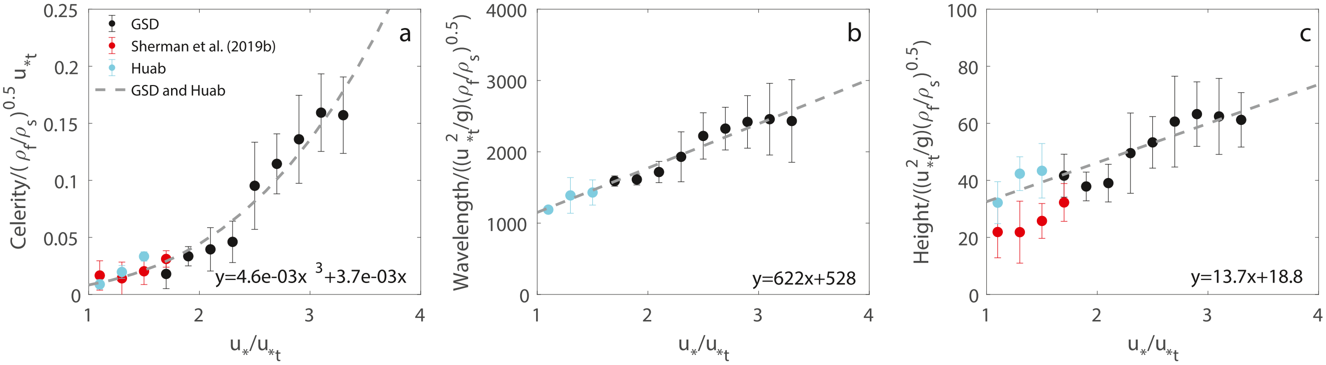

**Figure 2.** Normalized relationships between ripple (a) celerity, (b) wavelength, and (c) height and shear velocity, with comparisons to other data sets, where $g$ is gravity, $\rho_f$ is fluid density and $\rho_s$ is sediment density. Error bars indicate standard deviation within each normalized shear velocity bin. The $R^2$ values for dashed line fits are 0.95, 0.96, and 0.82 for ripple celerity, wavelength and height, respectively.

ripple relative to the mean surface height enables an increased shear velocity to be experienced on the ripple crest, acting to increase local erosion and ripple celerity. Alternatively, under strong winds, the system might be transitional from a saltation- to a collision-characterized transport regime, where saltating grains collide dominantly with other grains above, rather than on, the surface, thereby traveling higher and faster and increasing the sediment flux (Pähtz & Durán, 2020; Ralaiarisoa et al., 2020). It is unclear if the threshold to a collisional regime measured in the wind tunnel is similar to a field environment, and our shear velocity values are lower than those reported by Ralaiarisoa et al. (2020). However, the possible transition toward the collision regime is supported by our celerity fit (Figure 2a) that switches from linear to cubic for higher $u_*$. This is in agreement with the quartic sediment flux relationship reported in Pähtz and Durán (2020), where sediment flux is equivalent to the product of celerity and ripple height or wavelength (Duran et al., 2014; Jerolmack et al., 2006), with our height and wavelength relationships remaining linear (Figures 2b and 2c). The dynamics of mid-air collisions in saltation would accelerate ripple celerity due to a greater relative flux acting on the ripple surface. More work is required to investigate whether these, or other factors, might be responsible for the cubic response of ripple celerity with stronger winds.

### 3.2. Ripple Dynamics, Flux Indicators and Lagged Response to Changes in Wind Speed and Direction

When comparing the response of ripple celerity, height and wavelength to changes in shear velocity, we find that celerity is the first geometric attribute to respond and exhibits a mean lag of 2.3 ± 1.1 min (Table 3). These time scales of several minutes make physical sense as they are typically ca. 10–20 times larger than the initial growth times estimated by linear stability analysis in the numerical simulations of Duran et al. (2014). Ripple height is the second fastest attribute to respond with a mean lag of 5.6 ± 1.7 min, while ripple wavelength was the slowest to

**Table 3**
*Ripple Adjustment Times for Each Data Set, Identified by Strongest Positive Cross-Covariance Peak With Uncertainty Specified With ± Based on Cross-Covariance Peak Half Width*

| | | Adjustment time between $u_*$ and ripple attributes (minutes) | | | | |
|---|---|---|---|---|---|---|
| Site | $u_*$ | $c_r \times h_r$ | $c_r \times \lambda_r$ | $c_r$ | $h_r$ | $\lambda_r$ |
| Huab barchan 2014 | 0.290 ± 0.013 | 0 + 1.2 | 0 + 1.3 | 0 + 1.3 | 5 ± 2.5 | – |
| Huab dome 2016 part A | 0.298 ± 0.010 | 7 ± 1.7 | 7 ± 1.6 | 7 ± 1.8 | 2 ± 0.9 | 6 ± 0.3 |
| Huab dome 2016 part B | 0.333 ± 0.016 | 0 + 1.2 | 0 + 1.0 | 0 + 1.3 | 9 ± 1.2 | 22 ± 0.3 |
| Huab dome 2018 | 0.264 ± 0.011 | 2 ± 2.1 | 1 ± 2.8 | 1 ± 2.1 | 8 ± 5.2 | 10 ± 5.5 |
| GSD 30th March 2023 | 0.541 ± 0.06 | – | – | – | 4 ± 0.3 | 4 ± 0.7 |
| GSD 30th March 2023 part B | 0.536 ± 0.068 | 1 ± 0.7 | 1 ± 0.8 | 0 + 0.6 | 7 ± 0.9 | 4 ± 1.0 |
| GSD 3rd April 2023 | 0.533 ± 0.067 | 5 ± 0.3 | 5 ± 0.3 | 6 ± 1.3 | 4 ± 0.7 | 4 ± 0.5 |
| Mean Values | | 2.5 ± 1.1 | 2.3 ± 1.2 | 2.3 ± 1.3 | 5.6 ± 1.7 | 8.3 ± 1.4 |

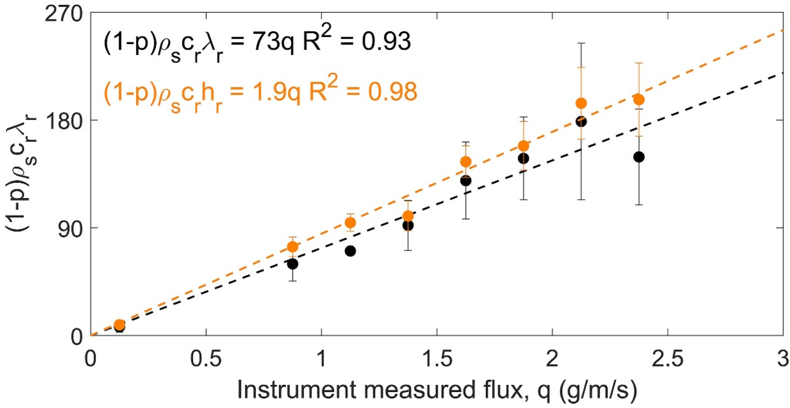

**Figure 3.** Comparison of wavelength-modeled and ripple height-modeled sediment flux to total field-measured flux, where *p* is porosity. Error bars indicate standard deviation within each measured flux bin.

respond to changes in wind speed (8.3 ± 1.4 min). In all data sets (both from GSD and the Huab), wavelength responded more slowly than either one or both celerity and height, irrespective of the magnitude of shear velocity or the variation in shear velocity driving the response (Table 3). This suggests that while ripple celerity is the most responsive indicator of shear velocity, ripple height is a better indicator of shear velocity than wavelength if wind conditions are fluctuating. Caution is thus advised when using wavelength as an indicator of shear velocity unless conditions have been consistent for ≥8 min, depending on the wind strength (Table 3). Furthermore, ripple morphometry might not represent the most recent wind conditions if the wind speed was reducing and there was insufficient time for the ripples to adjust.

Previous research has suggested that some function of ripple celerity, and either height (Jerolmack et al., 2006) or wavelength (Duran et al., 2014), could be used as a proxy to measure sediment flux. We find that either modeled flux method has a good linear relationship to measured flux (Figure 3; $R^2$ values of 0.98 and 0.93 for height and wavelength derived relationships, respectively). While these relationships both use ripple celerity and benefit from its faster response rate, the stronger $R^2$ value for the height relationship also infers that ripple height is a better indicator of sediment flux than wavelength.

The orientations of ripple crests were slower to respond to changes in wind direction than either height or celerity. The average response time for reorientation of a mature ripple crest to a change in wind direction was 6 min, depending on the magnitude of both the change in wind direction and the wind speed (Figure S2 in Supporting Information S1). Crestlines typically began to reorientate when the wind direction changed by more than 20°, in agreement with the observations of Sharp (1963).

These observed time lags have resonance with concepts of bedform turnover time seen in dune-scale patterns, where defect interactions are observed to be a key driver of pattern coarsening (e.g., Day & Kocurek, 2018; Ewing et al., 2006; Marvin et al., 2023, 2025; Werner & Kocurek, 1999). From this perspective, although ripple celerity is driven predominantly by wind speed, the changes in wavelength and orientation generated by adjustments in erosion and deposition, and defect interactions, mean that wavelengths, orientation and potentially height should adjust at a slower rate than celerity. While we recognize that in remote planetary locations and in the sedimentary record it is not possible to measure celerity, exploration of aeolian processes in planetary environments would benefit from high resolution temporal measurements in future missions to account for lags in ripple wavelength adjustments.

### 3.3. Saltation Height

We find that aerodynamic roughness increases over a sandy rippled surface with an increase in shear velocity (Figure 4a), in agreement with previous research (Field & Pelletier, 2018; Owen, 1964; Raupach, 1991; Sherman & Farrell, 2008). While both the Bagnold roughness equation (Equation 1) and Charnock equation (Equation 2) fit our data well ($R^2$ values of 0.9 and 0.89 respectively). We find that the best fit for the Charnock equation estimates a Charnock constant of 0.0155, which is closer to the wind tunnel value of $9.9 \times 10^{-3}$ of Sherman et al. (2019a) rather than Sherman et al. (2019a) field value of 0.085. This disparity may explain some of the mismatch between

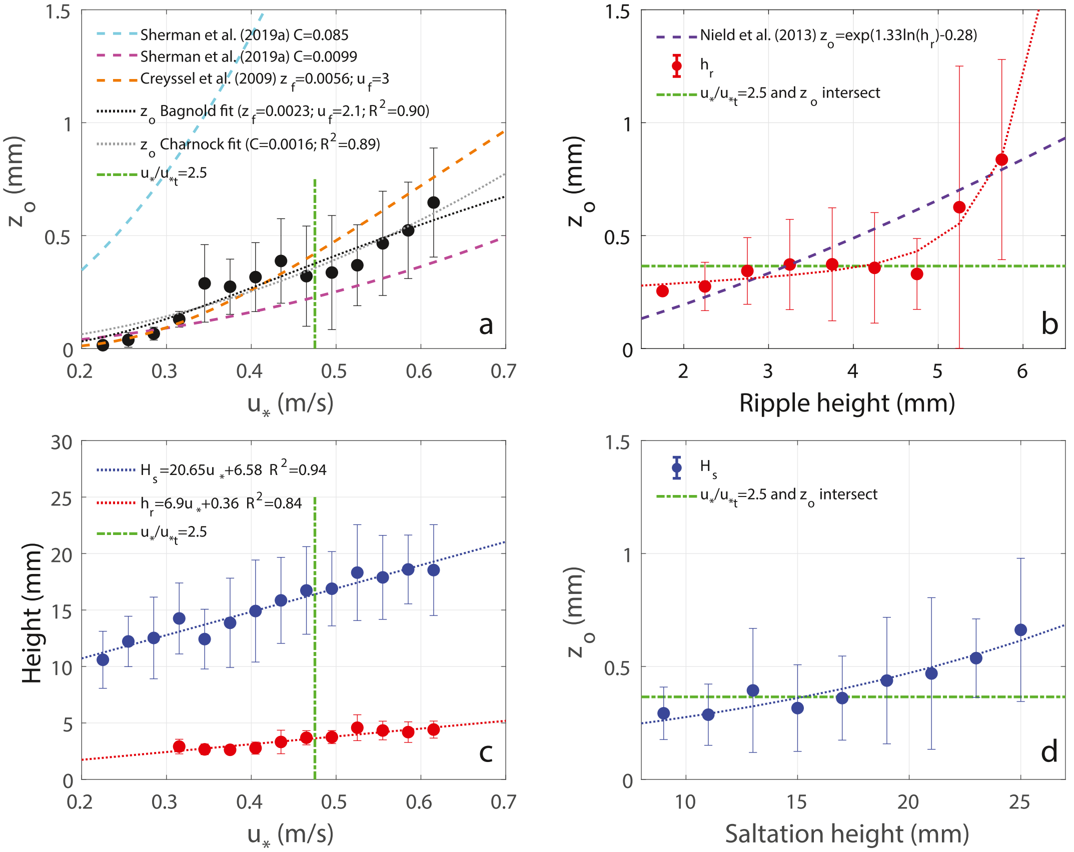

**Figure 4.** Variation of mean (a) aerodynamic roughness and (c) saltation and ripple height with changing shear velocity. Relationship between aerodynamic roughness and (b) ripple height and (d) saltation height. Error bars indicate standard deviation within each shear velocity, saltation, or ripple height bin. Green line identifies transition to the collision regime.

wind tunnel and field ripple relationships identified by Sherman et al. (2019a). Whilst it is recognized that there is a difference in how Law-of-the-Wall and Reynolds stress methods resolve $u_*$ (Lee & Baas, 2015), future studies of ripple dynamics should aim to undertake independent measurements of aerodynamic roughness and shear velocity rather than using a modeled aerodynamic roughness value. Using our relationship between $z_0$ and shear velocity, we can identify the value of aerodynamic roughness at which the transition to the collision regime begins ($u_*/u_{*_t} = 2.5$) to be approximately 0.365 mm, indicated by the green line in Figure 4.

Our data show that there is a small increase in saltation height with increased shear velocity (Figure 4c; $R^2 = 0.94$). Previous research has found that saltation height is invariant with changing shear velocity (as determined by profile measurements of sediment flux and low to moderate winds, Martin & Kok, 2017). However, high resolution TLS measurements of the full saltation height profile have shown small increases in maximum saltation height with increased shear velocity (Delorme et al., 2023), particularly during strong winds (Cohn et al., 2022) where saltation height is expected to increase due to collision theory (Ralaiarisoa et al., 2020).

We find that aerodynamic roughness increases with greater saltation height (Figure 4d), while changes in ripple height have a constant relationship with aerodynamic roughness. This confirms that saltation roughness drives the increase in aerodynamic roughness, as would be expected in a rough regime (Field & Pelletier, 2018). However, around a ripple height of ca. 0.0055 m, which corresponds to a $z_0$ value close to the modeled value of 0.365 mm when $u_*/u_{*_t} = 2.5$ (Figure 4b green line), we see a change in behavior with larger values of aerodynamic roughness. Above this value of ripple height, $z_0$ appears to match the value derived empirically for a surface of similar physical roughness in the absence of saltation (Nield et al., 2013). However, the standard deviation of saltation height over these larger ripples is also much greater (values greater than the green line, Figure 4d), demonstrating that these ripples may be submerged temporarily under transient sand streamers that would

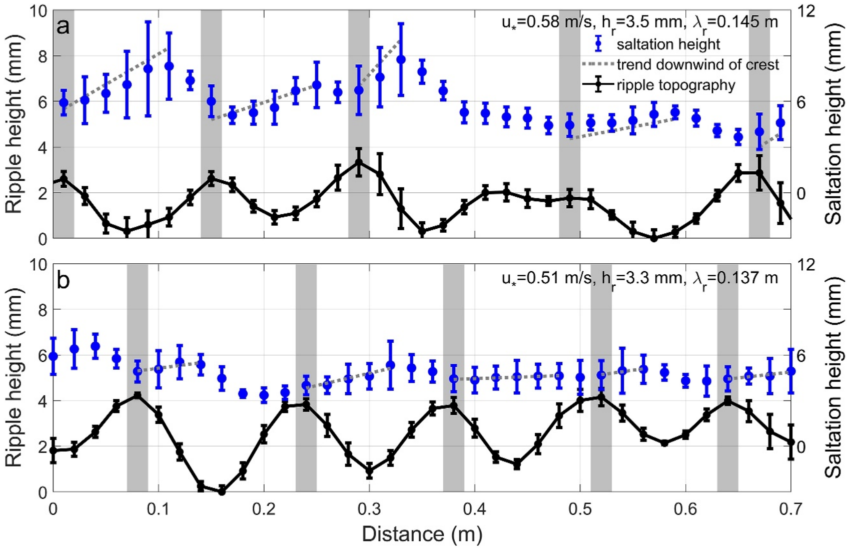

**Figure 5.** Examples of instantaneous saltation height over ripple topography on 30th March 2023, Great Sand Dunes National Park and Preserve. Shaded areas indicate the ripple crests. Peaks in saltation height occur 0.06 m downwind of the crest or 0.43 $\lambda_r$. With ripple height normalized by a cross covariance of 2.52 and 0.96 for (a) and (b), respectively.

variably increase the saltation height and collision potential. While more detailed studies are needed, these findings could also point to the movement of the system toward the collisional regime.

In stronger winds, it is also likely that saltation hop lengths will increase (Kok & Renno, 2009; Kok et al., 2012) and the relationship between increased hop length and ripple wavelength might not be in equilibrium due to the longer lag time response of wavelength as compared to height (Table 3). Our findings indicate that, in addition to a horizontal length scale, the vertical length scale of ripples and its relationship to saltation cloud height must be considered. This is needed in order to better parameterize inferred flow and flux relationships for aeolian ripples, particularly when flow, and therefore transport conditions, are changing temporally. The present results are the first to offer a way to disentangle the simultaneous influence of surface roughness (i.e., ripples) and saltation roughness (saltation height) on values of aerodynamic roughness ($z_0$) (Figures 4a–4d).

We identify field evidence for a difference in saltation dynamics over the stoss and lee slopes of ripples (Figure 5; Figure S3 in Supporting Information S1), in agreement with model (Anderson, 1987; Duran et al., 2014; Lester et al., 2025) and wind tunnel (Gordon & McKenna Neuman, 2011; Kelley, 2023; Kelley et al., 2025) results. On the stoss slope, we find generally smaller saltation heights relative to saltation heights on lee slopes, particularly in stronger winds (Figure S3 in Supporting Information S1), indicative of a greater splash density and more grain collision and ejection events over the stoss slopes (Anderson, 1987; Lester et al., 2025; Prigozhin, 1999). On the lee side, we find that the mean saltation heights are larger, likely because more grains bypass the lee slope (Allen, 1968; Duran et al., 2014). In the majority of cases, the initial increase in mean saltation height occurs at or immediately downwind of the ripple crest, with the peak in saltation height occurring approximately 0.43 $\lambda_r$ downwind of the ripple crest (Figure 5). This peak in saltation height over ripple troughs is more robust under stronger winds (cross covariance of 2.52 and 0.96 $h_r$ for $u_*$ values of 0.58 and 0.51 m/s respectively; Figure 5), as more grains are transported over the ripple topography and potentially lifted into saltation (Pähtz & Tholen, 2021). We also find that the standard deviation of saltation heights over the lee slope is greater (mean value of $5.1 \times 10^{-4}$ m vs. $4.5 \times 10^{-4}$ m; Figures 4c and 4d), indicative of a greater variation in fall trajectories over these more sheltered slopes. This increase in the variability of saltation height over ripples during stronger winds ($>2.5$ $u_*/u_{*t}$) may contribute to the greater variability of aerodynamic roughness over larger ripples discussed above (Figure 4b). Our results should help to parameterize models such as those of Lester et al. (2025) and Duran et al. (2014), where the modulation of saltation over ripples is important to quantify.

Future research should examine the dynamics of ripples over a greater range of grain sizes and wind regimes to extend our understanding of these self-organizing patterns (Anderson, 1990; Baas, 2002; Coco & Murray, 2007; Landry & Werner, 1994). Further, whilst our findings elucidate the key role of surface features and saltation trajectories in aeolian processes, more studies will help quantify how form-flow-saltation dynamics change under strong winds.

## 4. Conclusions

We find that ripple dynamics are good indicators of shear velocity and sediment flux, with ripple celerity possessing a stronger relationship with flow conditions than either ripple height or wavelength. Although ripple wavelength and height can also be used to infer flow conditions, ripple wavelength is slower to respond to changes in wind speed, particularly when wind speeds are decreasing; caution should be used when utilizing ripple wavelength to infer instantaneous flow conditions. This is significant because wavelength dimensions are often the only available data from contemporary planetary landscapes or derived from supercritically climbing aeolian ripples (sensu Hunter, 1977) within the rock record. In these instances, we suggest that wavelengths might not represent the full range of fluctuating wind conditions but rather approximate previous mean sediment transport conditions that were sustained for a long enough period of time that the ripples had fully adjusted. While ripple height and saltation height both increase with shear velocity, the impact of shear velocity on aerodynamic roughness—imparted by grains, sediment transport and form effects—is more nuanced. Critically, we also find a non-linear relationship between ripple celerity and shear velocity at high wind speeds. While a transition to a collision regime may in part help to explain both this non-linear celerity relationship and the switch from saltation height to ripple height as the key driver of aerodynamic roughness, more experiments are needed to test these hypotheses that capture coincident sediment transport and surface morphology for different grain sizes and wind conditions.

## Conflict of Interest

The authors declare no conflicts of interest relevant to this study.

## Data Availability Statement

All raw data and processing scripts (Nield, Baddock, et al., 2023; Nield, Wiggs, et al., 2023; Nield, Baddock, & Wiggs, 2025) along with processed ripple dynamics (Nield, Baddock, Wiggs, Best, et al., 2025) are available on the NERC EDS National Geoscience Data Centre, UK.

**Acknowledgments**

Funding is gratefully acknowledged from the National Geographic Society (GEFNE110-14 and CP-029R-17), British Society for Geomorphology, Natural Environment Research Council, UK and National Science Foundation, USA NSFGEO-NERC (NE/R010196/1; NSF 1829513; NSF 1829541; GEF-1025). The authors thank J. Mayaud, M. David, S. Muinjo, and B. Shiyanga for field assistance. We are grateful to the SoGES laboratory team who undertook the grain size analysis. We also acknowledge I. Matheus, J. Kazeurua, L. Uahengo, the Namibia Ministry of Environment and Tourism, NCRST and Skeleton Coast National Park Rangers for advice and site access (permits 1913/2014; 2051/2015; 2168/2016, RPIV00022018). F. Bunch was instrumental in the GSD fieldwork (permit GRSA-2018-SCI-004). J.M. Nield gratefully acknowledges the Department of Geology and Geophysics, Texas A&M University, where she was supported by a Michel T. Halbouty Visiting Chair during processing some of the data for this manuscript. Data processing was performed using the IRIDIS Southampton Computing Facility. We thank Joel Sankey, Mathieu Lapôtre, and two anonymous reviewers for their very useful comments that helped improve this manuscript.

## References

Allen, J. R. L. (1968). The diffusion of grains in the lee of ripples, dunes, and sand deltas. *Journal of Sedimentary Research*, *38*(2), 621–633. https://doi.org/10.1306/74D719FB-2B21-11D7-8648000102C1865D

Alvarez, C. A., Lapôtre, M. G. A., Swann, C., Ewing, R. C., Jia, P., & Claudin, P. (2025). Aerodynamic roughness of rippled beds under active saltation at Earth-to-Mars atmospheric pressures. *Nature Communications*, *16*(1), 5113. https://doi.org/10.1038/s41467-025-60212-7

Anderson, R. S. (1987). A theoretical model for aeolian impact ripples. *Sedimentology*, *34*(5), 943–956. https://doi.org/10.1111/j.1365-3091.1987.tb00814.x

Anderson, R. S. (1990). Eolian ripples as examples of self-organization in geomorphological systems. *Earth-Science Reviews*, *29*(1–4), 77–96. https://doi.org/10.1016/0012-8252(0)90029-U

Andreotti, B., Claudin, P., & Pouliquen, O. (2006). Aeolian Sand Ripples: Experimental study of fully developed states. *Physical Review Letters*, *96*(2), 028001. https://doi.org/10.1103/PhysRevLett.96.028001

Baas, A. C. W. (2002). Chaos, fractals and self-organization in coastal geomorphology: Simulating dune landscapes in vegetated environments. *Geomorphology*, *48*(1–3), 309–328. https://doi.org/10.1016/S0169-555X(02)00187-3

Bagnold, R. A. (1941). *The physics of blown sand and desert dunes*. Chapman and Hall. https://doi.org/10.1007/978-94-009-5682-7

Brown, S., Nickling, W. G., & Gillies, J. A. (2008). A wind tunnel examination of shear stress partitioning for an assortment of surface roughness distributions. *Journal of Geophysical Research*, *113*(F2), F02S06. https://doi.org/10.1029/2007JF000790

Cheng, H., Hayden, P., Robins, A. G., & Castro, I. P. (2007). Flow over cube arrays of different packing densities. *Journal of Wind Engineering and Industrial Aerodynamics*, *95*(8), 715–740. https://doi.org/10.1016/j.jweia.2007.01.004

Coco, G., & Murray, A. B. (2007). Patterns in the sand: From forcing templates to self-organization. *Geomorphology*, *91*(3–4), 271–290. https://doi.org/10.1016/j.geomorph.2007.04.023

Cohn, N., Dickhudt, P., & Brodie, K. (2022). Remote observations of aeolian saltation. *Geophysical Research Letters*, *49*(16), e2022GL100066. https://doi.org/10.1029/2022GL100066

Cooke, J. P., Jerolmack, D. J., & Park, G. I. (2025). The evolution of turbulence producing motions in the neutral ABL across a natural roughness transition. *Journal of Geophysical Research: Atmospheres*, *130*(5), e2024JD041768. https://doi.org/10.1029/2024JD041768

Creyssels, M., Dupont, P., El Moctar, A. O., Valance, A., Cantat, I., Jenkins, J. T., et al. (2009). Saltating particles in a turbulent boundary layer: Experiment and theory. *Journal of Fluid Mechanics*, *625*, 47–74. https://doi.org/10.1017/S0022112008005491

Davis, J. P., Walker, D. J., Townsend, M., & Young, I. R. (2004). Wave-formed sediment ripples: Transient analysis of ripple spectral development. *Journal of Geophysical Research*, *109*(C7), C07020. https://doi.org/10.1029/2004JC002307

Day, M., & Kocurek, G. (2018). Pattern similarity across planetary dune fields. *Geology*, *46*(11), 999–1002. https://doi.org/10.1130/g45547.1

Daynac, J., Bessin, P., Pochat, S., Mourgues, R., & Shumack, S. (2024). A new workflow for mapping dune features (outline, crestline and defects) combining deep learning and skeletonization from DEM-derived data. *Geomorphology*, *463*, 109369. https://doi.org/10.1016/j.geomorph.2024.109369

Delorme, P., Nield, J. M., Wiggs, G. F. S., Baddock, M. C., Bristow, N. R., Best, J. L., et al. (2023). Field evidence for the initiation of isolated aeolian sand patches. *Geophysical Research Letters*, *50*(4), e2022GL101553. https://doi.org/10.1029/2022GL101553

Duran, O., Andreotti, B., Claudin, P., & Winter, C. (2019). A unified model of ripples and dunes in water and planetary environments. *Nature Geoscience*, *12*(5), 345–350. https://doi.org/10.1038/s41561-019-0336-4

Duran, O., Claudin, P., & Andreotti, B. (2011). On aeolian transport: Grain-scale interactions, dynamical mechanisms and scaling laws. *Aeolian Research*, *3*(3), 243–270. https://doi.org/10.1016/j.aeolia.2011.07.006

Duran, O., Claudin, P., & Andreotti, B. (2014). Direct numerical simulations of aeolian sand ripples. *Proceedings of the National Academy of Sciences of the United States of America*, *111*(44), 15665–15668. https://doi.org/10.1073/pnas.1413058111

Ewing, R. C., Kocurek, G., & Lake, L. W. (2006). Pattern analysis of dune-field parameters. *Earth Surface Processes and Landforms*, *31*(9), 1176–1191. https://doi.org/10.1002/esp.1312

Ewing, R. C., Lapotre, M. G. A., Lewis, K. W., Day, M., Stein, N., Rubin, D. M., et al. (2017). Sedimentary processes of the Bagnold Dunes: Implications for the eolian rock record of Mars. *Journal of Geophysical Research: Planets*, *122*(12), 2544–2573. https://doi.org/10.1002/2017JE005324

Farrell, E. J., & Sherman, D. J. (2006). Process-scaling issues for aeolian transport modelling in field and wind tunnel experiments: Roughness length and mass flux distributions. *Journal of Coastal Research*, 384–389.

Field, J. P., & Pelletier, J. D. (2018). Controls on the aerodynamic roughness length and the grain-size dependence of aeolian sediment transport. *Earth Surface Processes and Landforms*, *43*(12), 2616–2626. https://doi.org/10.1002/esp.4420

Flack, K. A., & Schultz, M. P. (2010). Review of hydraulic roughness scales in the fully rough regime. *Journal of Fluids Engineering*, *132*(4), 041203. https://doi.org/10.1115/1.4001492

Furtak-Cole, E., Gillies, J. A., Hilgendorf, Z., Walker, I. J., & Nikolich, G. (2022). Simulation of flow and shear stress distribution on the Oceano Dunes, implications for saltation and dust emissions. *Environmental Fluid Mechanics*, *22*(6), 1399–1420. https://doi.org/10.1007/s10652-022-09902-0

Gillies, J. A., Nickling, W. G., & King, J. (2007). Shear stress partitioning in large patches of roughness in the atmospheric inertial sublayer. *Boundary-Layer Meteorology*, *122*(2), 367–396. https://doi.org/10.1007/s10546-006-9101-5

Gillies, J. A., Nickling, W. G., Nikolich, G., & Etyemezian, V. (2017). A wind tunnel study of the aerodynamic and sand trapping properties of porous mesh 3-dimensional roughness elements. *Aeolian Research*, *25*, 23–35. https://doi.org/10.1016/j.aeolia.2017.02.001

Goda, Y. (2000). *Random seas and design of maritime structures*. World Scientific. https://doi.org/10.1142/7425

Gordon, M., & McKenna Neuman, C. (2011). A study of particle splash on developing ripple forms for two bed materials. *Geomorphology*, *129*(1–2), 79–91. https://doi.org/10.1016/j.geomorph.2011.01.015

Ho, T. D., Valance, A., Dupont, P., & Ould El Moctar, A. (2011). Scaling laws in aeolian sand transport. *Physical Review Letters*, *106*(9), 094501. https://doi.org/10.1103/PhysRevLett.106.094501

Hood, D. R., Ewing, R. C., Roback, K. P., Runyon, K., Avouac, J. P., & McEnroe, M. (2021). Inferring airflow across Martian dunes from ripple patterns and dynamics. *Frontiers in Earth Science*, *9*, 702828. https://doi.org/10.3389/feart.2021.702828

Hugenholtz, C. H., & Barchyn, T. E. (2010). Spatial analysis of sand dunes with a new global topographic dataset: New approaches and opportunities. *Earth Surface Processes and Landforms*, *35*(8), 986–992. https://doi.org/10.1002/esp.2013

Hugenholtz, C. H., & Barchyn, T. E. (2011). Laboratory and field performance of a laser particle counter for measuring aeolian sand transport. *Journal of Geophysical Research*, *116*(F1), F01010. https://doi.org/10.1029/2010JF001822

Hunter, R. E. (1977). Basic types of stratification in small eolian dunes. *Sedimentology*, *24*(3), 361–387. https://doi.org/10.1111/j.1365-3091.1977.tb00128.x

Huo, X., Herrmann, H. J., Zhang, J., & Huang, N. (2024). Mid-air collisions control the wavelength of aeolian sand ripples. *Journal of Geophysical Research: Earth Surface*, *129*(4), e2023JF007365. https://doi.org/10.1029/2023JF007365

Jerolmack, D. J., Mohrig, D., Grotzinger, J. P., Fike, D. A., & Watters, W. A. (2006). Spatial grain size sorting in eolian ripples and estimation of wind conditions on planetary surfaces: Application to Meridiani Planum, Mars. *Journal of Geophysical Research*, *111*(E12), E12S02. https://doi.org/10.1029/2005JE002544

Jia, P., Andreotti, B., & Claudin, P. (2023). Hydrodynamic roughness induced by a multiscale topography. *Journal of Fluid Mechanics*, *974*, A16. https://doi.org/10.1017/jfm.2023.795

Kelley, M. (2023). *Re-evaluating the interactions between sand transport, wind, and ripples to improve aeolian sediment transport prediction*. Arizona State University. Retrieved from https://www.proquest.com/dissertations-theses/re-evaluating-interactions-between-sand-transport/docview/2851176609/se-2?accountid=13963

Kelley, M. M., Walker, I. J., Schmeeckle, M., Swann, C., Dorn, R., Roberts, M., & O'Brien, P. (2025). Changes in aeolian saltation cloud properties with wind speed and ripples. *Aeolian Research*, *74*, 100996. https://doi.org/10.1016/j.aeolia.2025.100996

King, J., Nickling, W. G., & Gillies, J. A. (2006). Aeolian shear stress ratio measurements within mesquite-dominated landscapes of the Chihuahuan Desert, New Mexico, USA. *Geomorphology*, *82*(3–4), 229–244. https://doi.org/10.1016/j.geomorph.2006.05.004

King, J., Nickling, W. G., & Gillies, J. A. (2008). Investigations of the law-of-the-wall over sparse roughness elements. *Journal of Geophysical Research*, *113*(F2), F02S07. https://doi.org/10.1029/2007JF000804

Kok, J. F., Parteli, E. J. R., Michaels, T. I., & Karam, D. B. (2012). The physics of wind-blown sand and dust. *Reports on Progress in Physics*, *75*(10), 106901. https://doi.org/10.1088/0034-4885/75/10/106901

Kok, J. F., & Renno, N. O. (2009). A comprehensive numerical model of steady state saltation (COMSALT). *Journal of Geophysical Research*, *114*(D17), D17204. https://doi.org/10.1029/2009JD011702

Lancaster, N., & Baas, A. (1998). Influence of vegetation cover on sand transport by wind: Field studies at Owens Lake, California. *Earth Surface Processes and Landforms*, *23*(1), 69–82. https://doi.org/10.1002/(sici)1096-9837(199801)23:1<69::aid-esp823>3.0.co;2-g

Landry, W., & Werner, B. T. (1994). Computer-simulations of self-organized wind ripple patterns. *Physica D*, *77*(1–3), 238–260. https://doi.org/10.1016/0167-2789(94)90137-6

Lapôtre, M. G. A., Ewing, R. C., & Lamb, M. P. (2021). An evolving understanding of enigmatic large ripples on Mars. *Journal of Geophysical Research: Planets*, *126*(2), e2020JE006729. https://doi.org/10.1029/2020JE006729

Lapotre, M. G. A., Ewing, R. C., Lamb, M. P., Fischer, W. W., Grotzinger, J. P., Rubin, D. M., et al. (2016). Large wind ripples on Mars: A record of atmospheric evolution. *Science*, *353*(6294), 55–58. https://doi.org/10.1126/science.aaf3206

Lee, Z. S., & Baas, A. C. W. (2015). Variable and conflicting shear stress estimates inside a boundary layer with sediment transport. *Earth Surface Processes and Landforms*, *41*(4), 435–445. https://doi.org/10.1002/esp.3829

Lester, C. W., Murray, A. B., Duran, O., Andreotti, B., & Claudin, P. (2025). Emergence of wind ripples controlled by mechanics of grain–bed impacts. *Nature Geoscience*, *18*(4), 344–350. https://doi.org/10.1038/s41561-025-01672-w

Liu, Z. Y. C., & Zimbelman, J. R. (2015). Recent near-surface wind directions inferred from mapping sand ripples on Martian dunes. *Icarus*, *261*, 169–181. https://doi.org/10.1016/j.icarus.2015.08.022

Lorenz, R. D. (2011). Observations of wind ripple migration on an Egyptian seif dune using an inexpensive digital timelapse camera. *Aeolian Research*, *3*(2), 229–234. https://doi.org/10.1016/j.aeolia.2011.01.004

Lorenz, R. D., & Valdez, A. (2011). Variable wind ripple migration at Great Sand Dunes National Park and Preserve, observed by timelapse imaging. *Geomorphology*, *133*(1–2), 1–10. https://doi.org/10.1016/j.geomorph.2011.06.003

Marticorena, B., & Bergametti, G. (1995). Modeling the atmospheric dust cycle: 1. Design of a soil-derived dust emission scheme. *Journal of Geophysical Research*, *100*(D8), 16415–16430. https://doi.org/10.1029/95JD00690

Martin, R. L., & Jerolmack, D. J. (2013). Origin of hysteresis in bed form response to unsteady flows. *Water Resources Research*, *49*(3), 1314–1333. https://doi.org/10.1002/wrcr.20093

Martin, R. L., & Kok, J. F. (2017). Wind-invariant saltation heights imply linear scaling of aeolian saltation flux with shear stress. *Science Advances*, *3*(6), e1602569. https://doi.org/10.1126/sciadv.1602569

Marvin, M. C., Lapôtre, M. G. A., Gunn, A., Day, M., & Soto, A. (2023). Dune interactions record changes in boundary conditions. *Geology*, *51*(10), 947–951. https://doi.org/10.1130/g51264.1

Marvin, M. C., Lapôtre, M. G. A., Radebaugh, J., & Bo, W. (2025). From Xanadu around and back: A ca. 11,000 km journey of windblown sand revealed by global dune patterns on Titan. *Geophysical Research Letters*, *52*(5), e2024GL112760. https://doi.org/10.1029/2024GL112760

Nield, J. M., Baddock, M. C., & Wiggs, G. F. S. (2025). Surface and meteorological data of ripples, saltation and protodune dynamics at Medano Creek, Great Sand Dunes National Park and Preserve, Colorado, USA in March and April 2023 [Dataset]. *NERC EDS National Geoscience Data Centre*. https://doi.org/10.5285/4b86b7a5-51ee-47b8-836d-a72cfd2be26b

Nield, J. M., Baddock, M. C., Wiggs, G. F. S., Best, J., Christensen, K. T., Delorme, P., et al. (2025). Form-flow-saltation dynamics of aeolian sand ripples at Medano Creek, Great Sand Dunes National Park and Preserve, Colorado, USA and the Huab Dune Field, Skeleton Coast, Namibia from 2014 to 2023 [Dataset]. *NERC EDS National Geoscience Data Centre*. https://doi.org/10.5285/3de63fc0-390f-451d-bcc1-c15e4ce78d40

Nield, J. M., Baddock, M. C., Wiggs, G. F. S., Delorme, P., Valdez, A., Wallum, N., & Goss, D. (2023). Surface and meteorological data of ripple and saltation dynamics at Medano Creek area, Great Sand Dunes National Park, Colorado, USA on 5-11th April 2022 [Dataset]. *NERC EDS National Geoscience Data Centre*. https://doi.org/10.5285/738dc233-3bd7-4174-aa98-8c33fc35f344

Nield, J. M., King, J., Wiggs, G. F. S., Leyland, J., Bryant, R. G., Chiverrell, R. C., et al. (2013). Estimating aerodynamic roughness over complex surface terrain. *Journal of Geophysical Research: Atmospheres*, *118*(23), 2013JD020632. https://doi.org/10.1002/2013JD020632

Nield, J. M., & Wiggs, G. F. S. (2011). The application of terrestrial laser scanning to aeolian saltation cloud measurement and its response to changing surface moisture. *Earth Surface Processes and Landforms*, *36*(2), 273–278. https://doi.org/10.1002/esp.2102

Nield, J. M., Wiggs, G. F. S., Baddock, M. C., & Delorme, P. (2023). Surface and meteorological data of saltation and ripple dynamics at Huab Dune Field, Skeleton Coast National Park, Namibia 2014, 2016 and 2018 [Dataset]. *NERC EDS National Geoscience Data Centre*. https://doi.org/10.5285/cc1b2bd9-2099-4fea-a731-6b4cf3d4c2be

Nikuradse, J. (1933). Laws of flow in rough pipes. In *NACA Technical Memorandum 1292*.

Owen, P. R. (1964). Saltation of uniform grains in air. *Journal of Fluid Mechanics*, *20*(2), 225–242. https://doi.org/10.1017/S0022112064001173

Pähtz, T., & Durán, O. (2020). Unification of aeolian and fluvial sediment transport rate from granular physics. *Physical Review Letters*, *124*(16), 168001. https://doi.org/10.1103/PhysRevLett.124.168001

Pähtz, T., & Durán, O. (2023). Scaling laws for planetary sediment transport from DEM-RANS numerical simulations. *Journal of Fluid Mechanics*, *963*, A20. https://doi.org/10.1017/jfm.2023.343

Pähtz, T., & Tholen, K. (2021). Aeolian sand transport: Scaling of mean saltation length and height and implications for mass flux scaling. *Aeolian Research*, *52*, 100730. https://doi.org/10.1016/j.aeolia.2021.100730

Pelletier, J. D., & Field, J. P. (2016). Predicting the roughness length of turbulent flows over landscapes with multi-scale microtopography. *Earth Surface Dynamics*, *4*(2), 391–405. https://doi.org/10.5194/esurf-4-391-2016

Prigozhin, L. (1999). Nonlinear dynamics of aeolian sand ripples. *Physical Review E*, *60*(1), 729–733. https://doi.org/10.1103/PhysRevE.60.729

Ralaiarisoa, J. L., Besnard, J. B., Furieri, B., Dupont, P., Ould El Moctar, A., Naaim-Bouvet, F., & Valance, A. (2020). Transition from saltation to collisional regime in windblown sand. *Physical Review Letters*, *124*(19), 198501. https://doi.org/10.1103/PhysRevLett.124.198501

Raupach, M. R. (1991). Saltation layers, vegetation canopies and roughness lengths. In *Paper presented at aeolian grain transport 1*. Springer Vienna.

Raupach, M. R. (1992). Drag and drag partition on rough surfaces. *Boundary-Layer Meteorology*, *60*(4), 375–395. https://doi.org/10.1007/BF00155203

Raupach, M. R., Gillette, D. A., & Leys, J. F. (1993). The effect of roughness elements on wind erosion threshold. *Journal of Geophysical Research*, *98*(D2), 3023–3029. https://doi.org/10.1029/92JD01922

Roback, K. P., Runyon, K., Newman, C., & Avouac, J. P. (2022). Multi-year measurements of ripple and dune migration on Mars: Implications for the wind regime and sand transport. *Icarus*, *380*, 114966. https://doi.org/10.1016/j.icarus.2022.114966

Rubanenko, L., Lapôtre, M. G. A., Ewing, R. C., Fenton, L. K., & Gunn, A. (2022). A distinct ripple-formation regime on Mars revealed by the morphometrics of barchan dunes. *Nature Communications*, *13*(1), 7156. https://doi.org/10.1038/s41467-022-34974-3

Seppälä, M., Lindé, K., Seppala, M., & Linde, K. (1978). Wind tunnel studies of ripple formation. *Geografiska Annaler—Series A: Physical Geography*, *60*(1/2), 29–42. https://doi.org/10.2307/520963

Shao, Y., Nickling, W., Bergametti, G., Butler, H., Chappell, A., Findlater, P., et al. (2015). A tribute to Michael R. Raupach for contributions to aeolian fluid dynamics. *Aeolian Research*, *19*(Part A), 37–54. https://doi.org/10.1016/j.aeolia.2015.09.004

Sharp, R. P. (1963). Wind ripples. *The Journal of Geology*, *71*(617), 636. https://doi.org/10.1086/626936

Sherman, D. J., & Farrell, E. J. (2008). Aerodynamic roughness lengths over movable beds: Comparison of wind tunnel and field data. *Journal of Geophysical Research*, *113*(F2), F02S08. https://doi.org/10.1029/2007JF000784

Sherman, D. J., Zhang, P., Martin, R. L., Ellis, J. T., Kok, J. F., Farrell, E. J., & Li, B. (2019a). Aeolian ripple migration and associated creep transport rates. *Geosciences*, *9*(9), 389. https://doi.org/10.3390/geosciences9090389

Sherman, D. J., Zhang, P., Martin, R. L., Ellis, J. T., Kok, J. F., Farrell, E. J., & Li, B. (2019b). Data for aeolian ripple migration and associated creep transport rates [Dataset]. *Zenodo*. https://doi.org/10.5281/zenodo.3378825

Silvestro, S., Fenton, L. K., Vaz, D. A., Bridges, N. T., & Ori, G. G. (2010). Ripple migration and dune activity on Mars: Evidence for dynamic wind processes. *Geophysical Research Letters*, *37*(20), L20203. https://doi.org/10.1029/2010GL044743

Sullivan, R., Kok, J. F., Katra, I., & Yizhaq, H. (2020). A broad continuum of aeolian impact ripple morphologies on Mars is enabled by low wind dynamic pressures. *Journal of Geophysical Research: Planets*, *125*(10), e2020JE006485. https://doi.org/10.1029/2020JE006485

Uphues, C. F. K., van Ijzendoorn, C. O., Hallin, C., Pearson, S. G., van Prooijen, B. C., Miot da Silva, G., & de Vries, S. (2022). Coastal aeolian sediment transport in an active bed surface layer: Tracer study and conceptual model. *Earth Surface Processes and Landforms*, *47*(13), 3147–3162. https://doi.org/10.1002/esp.5449

Valance, A., Rasmussen, K. R., Ould El Moctar, A., & Dupont, P. (2015). The physics of aeolian sand transport. *Comptes Rendus Physique*, *16*(1), 105–117. https://doi.org/10.1016/j.crhy.2015.01.006

van Boxel, J. H., Sterk, G., & Arens, S. M. (2004). Sonic anemometers in aeolian sediment transport research. *Geomorphology*, *59*(1–4), 131–147. https://doi.org/10.1016/j.geomorph.2003.09.011

Van Pelt, R. S., Peters, P., & Visser, S. (2009). Laboratory wind tunnel testing of three commonly used saltation impact sensors. *Aeolian Research*, *1*(1), 55–62. https://doi.org/10.1016/j.aeolia.2009.05.001

Vaz, D. A., Silvestro, S., Chojnacki, M., & Silva, D. C. A. (2023). Constraining the mechanisms of aeolian bedform formation on Mars through a global morphometric survey. *Earth and Planetary Science Letters*, *614*, 118196. https://doi.org/10.1016/j.epsl.2023.118196

Werner, B. T., Haff, P. K., Livi, R. P., & Anderson, R. S. (1986). Measurement of eolian sand ripple cross-sectional shapes. *Geology*, *14*(9), 743–745. https://doi.org/10.1130/0091-7613(1986)14<743:Moesrc>2.0.Co;2

Werner, B. T., & Kocurek, G. (1999). Bedform spacing from defect dynamics. *Geology*, *27*(8), 727–730. https://doi.org/10.1130/0091-7613(1999)027<0727:Bsfdd>2.3.Co;2

Wolfe, S. A., & Nickling, W. G. (1996). Shear stress partitioning in sparsely vegetated desert canopies. *Earth Surface Processes and Landforms*, *21*(7), 607–619. https://doi.org/10.1002/(SICI)1096-9837(199607)21:7<607::AID-ESP660>3.0.CO;2-1

Yizhaq, H., Balmforth, J., & Provenzale, A. (2004). Blown by wind: Nonlinear dynamics of aeolian sand ripples. *Physica D: Nonlinear Phenomena*, *195*(3–4), 207–228. https://doi.org/10.1016/j.physd.2004.03.015

Yizhaq, H., Isenberh, O., Wenkart, R., Tsoar, H., & Karnieli, A. (2008). Morphology and dynamics of aeolian mega-ripples in Nahal Kasuy, southern Israel. *Israel Journal of Earth Sciences*, *57*(3–4), 149–165. https://doi.org/10.1560/IJES.57.3–4.149

Yizhaq, H., Tholen, K., Saban, L., Swet, N., Lester, C., Silvestro, S., et al. (2024). Coevolving aerodynamic and impact ripples on Earth. *Nature Geoscience*, *17*(1), 66–72. https://doi.org/10.1038/s41561-023-01348-3

Zimbelman, J. R., Williams, S. H., & Johnston, A. K. (2012). Cross-sectional profiles of sand ripples, megaripples, and dunes: A method for discriminating between formational mechanisms. *Earth Surface Processes and Landforms*, *37*(10), 1120–1125. https://doi.org/10.1002/esp.3243

## References From the Supporting Information

Baddock, M. C., Nield, J. M., & Wiggs, G. F. S. (2018). Early-stage aeolian protodunes: Bedform development and sand transport dynamics. *Earth Surface Processes and Landforms*, *43*(1), 339–346. https://doi.org/10.1002/esp.4242

Baddock, M. C., Wiggs, G. F. S., & Livingstone, I. (2011). A field study of mean and turbulent flow characteristics upwind, over and downwind of barchan dunes. *Earth Surface Processes and Landforms*, *36*(11), 1435–1448. https://doi.org/10.1002/esp.2161

Martin, R. L., & Kok, J. F. (2018). Distinct thresholds for the initiation and cessation of aeolian saltation from field measurements. *Journal of Geophysical Research: Earth Surface*, *123*(7), 1546–1565. https://doi.org/10.1029/2017JF004416

Mayaud, J. R., Bailey, R. M., Wiggs, G. F. S., & Weaver, C. M. (2017). Modelling aeolian sand transport using a dynamic mass balancing approach. *Geomorphology*, *280*, 108–121. https://doi.org/10.1016/j.geomorph.2016.12.006

Nield, J. M. (2011). Surface moisture induced feedback in aeolian environments. *Geology*, *39*(10), 915–918. https://doi.org/10.1130/G32151.1

Ungar, J. E., & Haff, P. K. (1987). Steady state saltation in air. *Sedimentology*, *34*(2), 289–299. https://doi.org/10.1111/j.1365-3091.1987.tb00778.x

Weaver, C. M. (2008). *Turbulent flow and sand dune dynamics: Identifying controls on aeolian sediment transport* [DPhil Thesis]. University of Oxford.

Weaver, C. M., & Wiggs, G. F. S. (2011). Field measurements of mean and turbulent airflow over a barchan sand dune. *Geomorphology*, *128*(1–2), 32–41. https://doi.org/10.1016/j.geomorph.2010.12.020